

> REPLACE THIS LINE WITH YOUR MANUSCRIPT ID NUMBER (DOUBLE-CLICK HERE TO EDIT) <

# Terahertz Dual-Band Metamaterial Biosensor for Cervical-Cancer Diagnostics

Musa N. Hamza, Mohammad Alibakhshikenari, Bal Virdee, Muhamad A. Hamad, Salahuddin Khan, Slawomir Koziel, and Ernesto Limiti

**Abstract**— This study highlights the potential of employing terahertz metamaterial structures as dual-band biosensors for the early detection of cancerous biological tissue. The fundamental principle leveraged here is the alteration of the effective dielectric constant of biological tissue by cancerous cells. The change in the dielectric constant, in turn, induces a shift in the resonance frequency of the metamaterial sensor. One notable advantage of the terahertz metamaterial sensor is its relatively compact size compared to other sensor types, as its dimensions are independent of the wavelength. This property translates into a requirement for a much smaller biopsy sample, facilitating less invasive testing procedures. Beyond the size advantage, the proposed biosensor demonstrates efficacy in detecting abnormalities within biological tissue.

**Index Terms**— Biosensors; terahertz; metamaterials; cancer

## I. INTRODUCTION

The World Health Organization (WHO) estimates that approximately 10 million people worldwide died from cancer in 2020. Cancer is a complex disease that affects various bodily systems, characterized by the uncontrolled growth of abnormal cells. These malignant cells have the potential to cause organ failure and death. However, early identification and prompt treatment of these malignant cells could significantly improve survival rates, especially for breast cancer patients [1].

The authors sincerely appreciate funding from Researchers Supporting Project number (RSP2024R58), King Saud University, Riyadh, Saudi Arabia. This work is partially supported by the Icelandic Research Fund Grant 2410297 and by National Science Centre of Poland Grant 2022/47/B/ST7/00072.

Musa N. Hamza, Mohammad Alibakhshikenari and Ernesto Limiti are the *Corresponding Authors*.

Musa N. Hamza is with Department of Physics, College of Science, University of Raparin, Sulaymaniyah 46012, Iraq. (e-mail: [musa.nuraden@uor.edu.krd](mailto:musa.nuraden@uor.edu.krd))

Mohammad Alibakhshikenari and Ernesto Limiti are with the Electronics Engineering Department, University of Rome "Tor Vergata", 00133 Rome, Italy. (e-mail: [mohammad.alibakhshikenari@uc3m.es](mailto:mohammad.alibakhshikenari@uc3m.es) and [limiti@ing.uniroma2.it](mailto:limiti@ing.uniroma2.it))

Bal Virdee is with Department of Center for Communications Technology, London Metropolitan University, London N7 8DB, United Kingdom; (e-mail: [b.virdee@londonmet.ac.uk](mailto:b.virdee@londonmet.ac.uk))

Muhamad A. Hamad is with Physics Department, College of Education, Salahaddin University, Erbil 44002, Iraq. (e-mail: [muhamad.hamad@su.edu.krd](mailto:muhamad.hamad@su.edu.krd))

Salahuddin Khan is with College of Engineering, King Saud University, P.O.Box 800, Riyadh 11421, Saudi Arabia; (e-mail: [drskhan@ksu.edu.sa](mailto:drskhan@ksu.edu.sa))

Slawomir Koziel is with the Engineering Optimization & Modeling Center, Reykjavik University, 102 Reykjavik, Iceland, and also with the Faculty of Electronics, Telecommunications and Informatics, Gdansk University of Technology, 80-233 Gdansk, Poland (e-mail: [koziel@ru.is](mailto:koziel@ru.is))

Currently, traditional methods such as physical examinations, hematology analyses, ultrasound imaging, histopathology, and cytology are the primary means of early cancer detection. While these methods can enhance patient survival and cure rates, they often come with adverse side effects. Imaging techniques such as computed tomography (CT) scans emit substantial radiation, increasing the risk of cancer. Magnetic resonance imaging (MRI) and positron emission tomography (PET) scans, although effective, are often not accessible due to high associated costs [2]. Additionally, blood tests for tumor detection may be less effective in certain types of cancer due to the lack of relevant blood-based biomarkers. Consequently, researchers are focusing on developing biosensors for early disease detection [2].

Cervical cancer is the fourth most common cancer in women worldwide and the leading cause of female cancer-related deaths. Recognizing the importance of early detection and precise diagnosis in improving patient outcomes and reducing mortality rates, addressing this challenge is of paramount importance. Cervical cancer is highly prevalent, especially in resource-limited regions, where limited access to healthcare facilities and diagnostic tools exacerbates the problem. The disease is strongly associated with modifiable risk factors, particularly persistent human papillomavirus (HPV) infection.

Despite significant advances in cervical cancer prevention and control, such as HPV vaccination, cervical cancer remains a prevalent and potentially lethal disease. Therefore, the development of improved diagnostic tools, especially those adaptable and feasible in diverse healthcare settings, is crucial [1] [3].

In the field of biosensing and diagnostics, the terahertz (THz) region, spanning from 0.1 to 10 THz, remains relatively unexplored. THz waves possess unique properties that make them ideal for biomedical applications, including low tissue absorption, a low ionization threshold, and the ability to interact with molecular structures. These properties open up opportunities for creating highly sensitive and precisely targeted biosensors with the potential to revolutionize disease diagnosis, including cervical cancer [4].

Metamaterials, artificially synthesized structures with exceptional optical properties surpassing those of natural materials, are critical in this context [5]. By engineering their unit structures, it is possible to modulate the electromagnetic response of incident waves and enhance interaction with the substance being measured on the metamaterial's surface. This interaction is most pronounced when the metamaterial's resonant frequency aligns with the characteristic frequency of

> REPLACE THIS LINE WITH YOUR MANUSCRIPT ID NUMBER (DOUBLE-CLICK HERE TO EDIT) <

the substance being measured. Terahertz metamaterial sensors are becoming a significant focus of research, benefiting from advancements in micro/nano fabrication [6].

Metamaterial-based sensors have garnered significant attention in recent years due to their unique ability to manipulate electromagnetic waves in ways not possible with natural materials. These artificially engineered structures possess subwavelength features that enable them to exhibit extraordinary electromagnetic properties, such as negative refractive index and enhanced light-matter interactions. One of the key advantages of metamaterial-based sensors is their ability to achieve high sensitivity and specificity in detecting minute changes in the surrounding environment, making them highly suitable for applications in biomedical diagnostics, environmental monitoring, and chemical detection. For instance, Liu et al. in [7] demonstrated a terahertz metamaterial biosensor capable of detecting protein molecules at picomolar concentrations by exploiting the strong localized electromagnetic fields generated by the metamaterial structure. Similarly, Landy et al. in [8] showcased a metamaterial-based perfect absorber that operates at microwave frequencies, which can be tuned to detect small changes in dielectric properties, highlighting the versatility of these sensors. The ability of metamaterials to support high-Q resonances, as explored by Al-Naib et al. in [9], further enhances their application in sensing, allowing for the precise detection of subtle variations in the refractive index of the surrounding medium. These features make metamaterial-based sensors a powerful tool in advancing sensing technologies across various fields.

Consequently metamaterial-based biosensors have also emerged as promising platforms for early disease detection due to their ability to manipulate electromagnetic waves at subwavelength scales. Recent studies have demonstrated the potential of incorporating quasi-bound states in the continuum (QBIC) into metasurface designs to enhance light-matter interactions and improve biosensing performance [10]. By leveraging QBIC resonances, these sensors can achieve increased sensitivity and specificity in detecting biomarkers associated with diseases such as cancer. However, addressing the complexities of biological samples remains a significant challenge in terahertz biosensing. The three-step one-way model proposed by [11] offers a systematic approach to overcoming issues related to sample heterogeneity and interference. By integrating this model with metamaterial-based biosensors, it is possible to develop robust and reliable diagnostic tools for early disease detection.

The concept of achieving high Q-factor resonances through metamaterial design, as demonstrated in [12], is crucial for enhancing the sensitivity and specificity of biosensors. High Q-factors allow metamaterial-based sensors to detect subtle changes in the surrounding medium more effectively. While the primary focus of [12] is on refractive index sensing, the underlying principles of metamaterial design for achieving high Q-factor resonances can be adapted for biosensing applications.

In cancer diagnosis, where different types and stages are characterized by unique biomarkers and molecular profiles, traditional single-frequency biosensors often struggle to capture this complexity. To enhance sensitivity and accuracy,

we have developed a dual-band biosensor based on metamaterial (MTM) technology. This biosensor shows great promise in addressing the heterogeneity of cancer types and stages by detecting these unique biomarkers. The numerical model used in this study is based on the well-established Finite Difference Time Domain (FDTD) technique, implemented through CST Microwave Studio Suite—an electromagnetic simulation tool widely recognized for its precision and accuracy, consistently validated by strong correlations with experimental results.

In summary, this study demonstrates the feasibility and advantages of using terahertz (THz) metamaterial structures as biosensors. These structures can detect early signs of cancer through resonance frequency modulation, highlighting their potential to improve diagnostic procedures with reduced invasiveness.

## II. METAMATERIAL UNIT CELL

The construction of biosensors is complicated and limited by the need for high sensitivity and specificity. Therefore, it is important to enhance the performance of biosensors to improve clinical performance and provide useful information for cervical cancer diagnosis. The proposed biosensor design will consider enhancing the accuracy which is necessary to provide reliable diagnosis of cervical cancer.

Figs. 1(a) and 1(b) illustrate a conceptual model, referred to as model#1, representing a metamaterial absorber designed for sensing applications. Fig. 1(c) introduces model#2. The integration of model#1 with model#2 results in the formation of a perfect metamaterial absorber, model#3, as depicted in Fig. 2(b). This strategic combination creates two distinct bands within the terahertz frequency range. The composite absorber consists of a dielectric metamaterial layer sandwiched between conductive layers. The key parameters defining the characteristics of these models are detailed in Table 1. The structure was optimized using a comprehensive full-wave 3D electromagnetic solver, CST Microwave Studio Suite by Dassault Systèmes.

TABLE 1: OPTIMIZED PHYSICAL PARAMETERS OF THE METAMATERIAL SENSOR.

Parameter	Value (μm)	Parameter	Value (μm)
A	150	I	84
B	150	J	44
C	15.6	K	44
D	23.5	Sensor thickness (T1) (see Fig.17)	10
E	2.6	Coverslip thickness (T2) (see Fig.17)	1
F	74	HeLa Cells thickness (T3) (see Fig.17)	7
G	103	Aluminum (Al) thickness	0.2
H	103		

Quantitative calculations are employed to analyze the properties of metamaterials and elucidate their behavior across varying frequency and size ranges. The literature extensively documents the investigation of different configurations,

> REPLACE THIS LINE WITH YOUR MANUSCRIPT ID NUMBER (DOUBLE-CLICK HERE TO EDIT) <

including unit cells, empty spaces, periodic arrays, and perfect electric and magnetic conductors (PEC and PMC) [7]-[9].

To streamline simulation processes, a unit cell was defined in the  $x$ - and  $y$ -directions, while an open space was incorporated in the  $z$ -direction. The three-layered model comprises a dielectric spacer at its core, composed of polyethylene terephthalate (PET), flanked by two Aluminum (Al) layers of  $0.2 \mu\text{m}$  thickness. PET is characterized by a low electrical conductivity of approximately  $1 \times 10^{12} \text{ S/m}$ , reflecting its insulating properties. The thickness of the dielectric spacer used is  $10 \mu\text{m}$ . To optimize performance, one of the Al layers needs to be engineered to exhibit an impedance compatible with the incident medium, facilitating maximum power penetration into and dispersion throughout the PET. Concurrently, the other Al layer serves as a barrier, designed to block all incident electromagnetic (EM) waves and eliminate transmission line interference (TLT). Electromagnetic waves transmitted through the model are terminated at a port featuring high electrical and/or magnetic loss. Through subjecting the model to electromagnetic waves, the absorption parameters of the model can be systematically determined and evaluated.

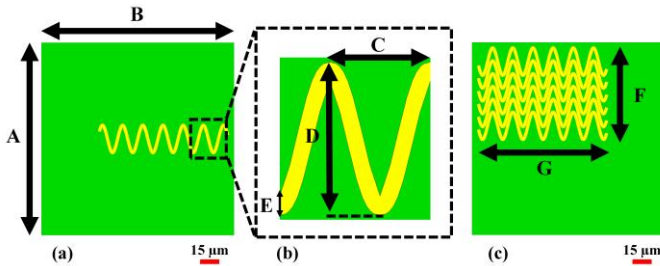


Fig. 1: Proposed metamaterial model#1 of a perfect absorber showing a single wave; (a) one wave, (b) one  $\lambda$ , and (c) model#2.

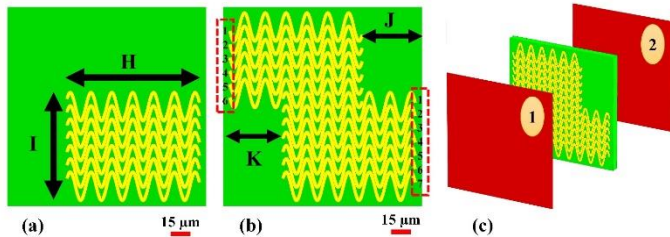


Fig. 2: A perfect metamaterial absorber; (a) model#1, (b) the proposed biosensor model#3, and (c) the proposed model#3 biosensor with input and output ports.

PET was selected for its optimal combination of dielectric, mechanical, and thermal properties, as well as its biocompatibility and cost-effectiveness. These attributes ensure minimal signal loss, maintain structural integrity, and enable safe interaction with biological tissues, thereby facilitating the sensor's reliable and efficient operation in various conditions.

In this study, the FDTD technique was employed for numerical modeling using CST Microwave Studio Suite. Accurate material properties were utilized to characterize the metamaterial unit cell at terahertz frequencies. Aluminum (Al) was chosen as the conductive material, with an electrical conductivity of  $3.77 \times 10^7 \text{ S/m}$ . The frequency-dependent permittivity of Aluminum was modeled using the Drude

model, which describes the material's response to electromagnetic waves and is defined by the following equation [13]:

$$\epsilon(\omega) = \epsilon_{\infty} - \frac{\omega_p^2}{\omega^2 + i\gamma\omega} \quad (1)$$

Where  $\epsilon(\infty)$  is the high-frequency permittivity,  $\omega_p$  is the plasma frequency,  $\gamma$  is the collision frequency, and  $\omega$  is the angular frequency.

Key parameters included a plasma frequency of  $2.24 \times 10^{15} \text{ rad/s}$  and a collision frequency of  $1.22 \times 10^{14} \text{ rad/s}$ , which are essential for accurately capturing the behavior of metals at terahertz frequencies.

The feasibility of the proposed biosensor relies on the integration of advanced materials, fabrication techniques, and computational modeling. By leveraging established metamaterial principles, the design achieves a compact form factor suitable for integration into existing diagnostic platforms. As will be shown later, the careful selection of materials and optimization through simulation have resulted in a device with high sensitivity and specificity, highlighting its potential for clinical application.

### III. RESULTS AND DISCUSSION

The expression used for modeling wave absorption in the biosensor within CST Microwave Studio Suite was:

$$A = 1 - R - T = 1 - |S_{11}|^2 - |S_{21}|^2 \quad (2)$$

The  $S$ -parameters for reflection and transmission are denoted by  $S_{11}$  and  $S_{21}$ , respectively. The reflection coefficient should be kept as low as possible to achieve maximal absorption.

To investigate the impact of resonator design on absorption capacity within the terahertz (THz) region, we examined twelve distinct models, as shown in Figs. 3 through 7. This exploration is essential for understanding the behavior and efficiency of THz metamaterials as perfect absorbers, requiring thorough characterization and performance assessment. The detailed analysis of these models provides valuable insights into the factors influencing signal resonance at various THz frequencies. This knowledge is crucial for refining design and manufacturing processes to achieve the desired absorption characteristics within this frequency range.

The first model, depicted in Fig. 3(a), exhibits two peaks at approximately  $0.437 \text{ THz}$  and  $0.75 \text{ THz}$ , with absorption rates exceeding  $99.7\%$  and  $98.4\%$ , respectively. In contrast, the second model, shown in Fig. 3(b), displays a single peak around  $0.65 \text{ THz}$ , achieving over  $98\%$  absorption. The third model, illustrated in Fig. 4(a), features a solitary peak at approximately  $0.65 \text{ THz}$  with an absorption rate above  $90\%$ . Similarly, the fourth model, shown in Fig. 4(b), has a single peak at about  $0.63 \text{ THz}$ , also surpassing  $90\%$  absorption.

The fifth model, depicted in Fig. 5(a), presents a single peak near  $0.5 \text{ THz}$ , achieving more than  $99\%$  absorption. The sixth model, shown in Fig. 5(b), incorporates two split-ring resonators, resulting in four peaks at around  $0.65 \text{ THz}$ ,  $0.75 \text{ THz}$ ,  $0.9 \text{ THz}$ , and  $1 \text{ THz}$ . However, this model does not reach perfect absorption, with an overall capacity below  $80\%$ .

> REPLACE THIS LINE WITH YOUR MANUSCRIPT ID NUMBER (DOUBLE-CLICK HERE TO EDIT) <

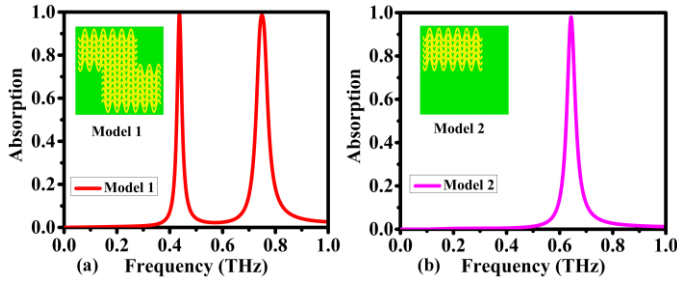


Fig. 3: Absorption spectra of the two designs: (a) Model#1, and (b) Model#2.

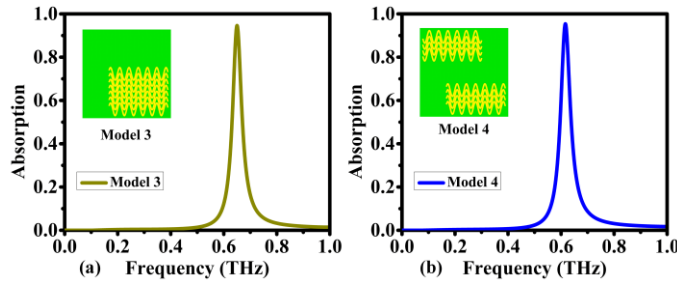


Fig. 4: Absorption spectra of the two designs: (a) Model#3, and (b) Model#4.

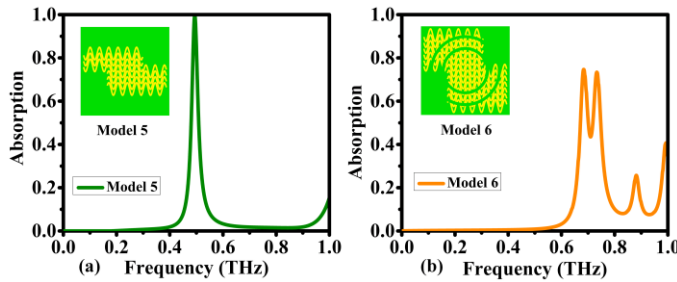


Fig. 5: Absorption spectra of the two designs: (a) Model#5, and (b) Model#6.

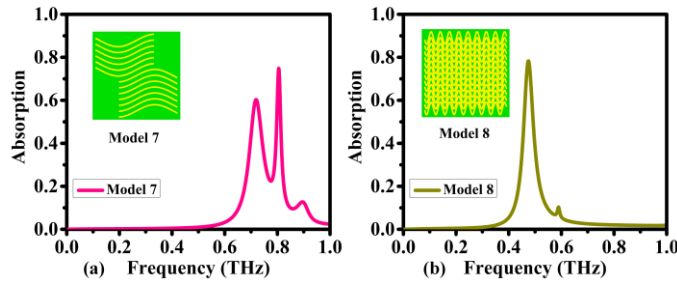


Fig. 6: Absorption spectra of the two designs: (a) Model#7, and (b) Model#8.

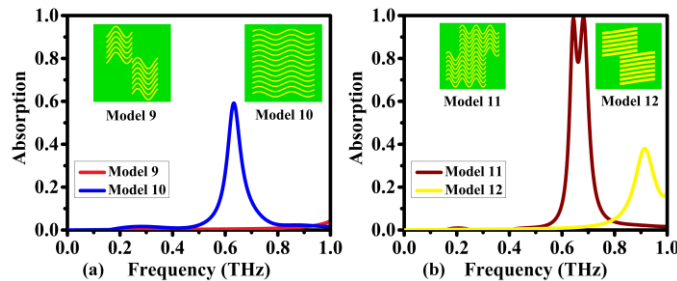


Fig. 7: Absorption spectra of the two designs: (a) Models#9 & #10, and (b) Models#11 & #12.

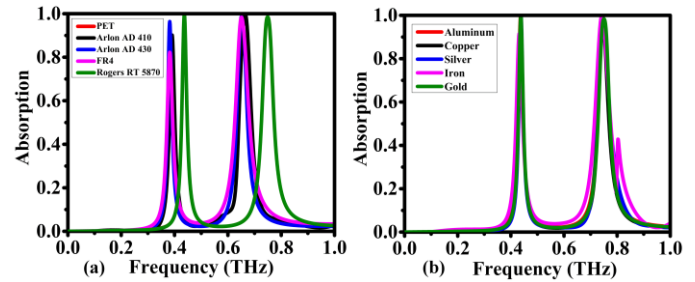


Fig. 8: Absorption spectra of the models: (a) using different substrate materials, and (b) using different metals as resonators.

The seventh model, shown in Fig. 6(a), reveals two peaks at approximately 0.7 THz and 0.8 THz, while the eighth model in Fig. 6(b) shows a single peak at around 0.5 THz. Both models, despite their peak counts, fail to meet the criteria for perfect absorption, with absorption capacities remaining below 80%.

The ninth and tenth models, depicted in Fig. 7, each exhibit a singular peak around 0.65 THz but do not achieve the threshold for perfect absorption at 80%. The eleventh model, shown in Fig. 7(a), resonates at around 0.63 THz and 0.72 THz, with absorption rates surpassing 98% and 99%, respectively. However, the proximity of these peaks introduces low resolution in microwave imaging, making it unsuitable for distinguishing healthy cells from malignant ones. Finally, the twelfth model, shown in Fig. 7(b), resonates at approximately 0.92 THz but falls short of perfect absorption, with a capacity below 80%.

Fig. 8 demonstrates the impact of substrate and resonator materials on the biosensor's absorption spectrum. The choice of substrate significantly influences resonant behaviour by altering the effective permittivity, which is a measure of how the material polarizes in response to an electric field. This change in effective permittivity modifies the resonance frequency by affecting the propagation speed and wavelength of electromagnetic waves within the sensor, which in turn impacts the peak absorption and bandwidth. A higher effective permittivity typically lowers the resonance frequency, leading to a shift in the absorption spectrum. The conductivity and plasmonic properties of the resonator material play a crucial role in determining the sharpness of the peaks and the intensity of the local electromagnetic fields. Materials with high conductivity and strong plasmonic activity, such as noble metals, support pronounced surface plasmon resonances, resulting in sharper and more intense absorption peaks. These factors collectively influence the biosensor's sensitivity, as the ability to detect subtle changes in the biological environment relies on these sharp, well-defined resonance peaks. By carefully selecting the substrate and resonator materials, the biosensor's performance can be optimized for high sensitivity and specificity, crucial for effective cancer diagnosis.

Several dielectric substrates were evaluated as potential candidates for the metamaterial absorber, including PET, Arlon AD 410, Arlon AD 430, FR-4, and Rogers RT5780. The absorption spectra for these materials are shown in Fig. 8(a). As expected, FR-4 performed comparatively poorly, as it is more suitable for low-frequency applications.

> REPLACE THIS LINE WITH YOUR MANUSCRIPT ID NUMBER (DOUBLE-CLICK HERE TO EDIT) <

The study also investigated the impact of different metals on the resonators, considering Aluminium, Copper, Silver, Iron, and Gold. The results, depicted in Fig. 8(b), show minimal variation in absorption characteristics among the metals, except for Iron, which introduced a small third resonance near the second peak. Overall, the choice of metal has a limited impact on the resonator's absorption characteristics, with Iron being the notable exception.

The absorption rate was evaluated across different incident and polarization angles, revealing how changes in angle affect the resonance conditions. Fig. 9 illustrates the biosensor's angular sensitivity and polarization dependence, which are influenced by the underlying physics of permittivity, resonance, and plasmonics. The effective permittivity of the substrate and the plasmonic properties of the resonator material play a crucial role in this behavior. Variations in incident angle alter the phase matching conditions, which can shift the resonance frequency and affect the intensity of absorption peaks. Similarly, the polarization of light impacts the coupling efficiency with surface plasmon resonances, with certain polarizations enhancing or diminishing the local electromagnetic fields. Consistent performance across these varying angles, as demonstrated in the results, indicates that the biosensor maintains stable resonance behavior and strong plasmonic responses under diverse experimental conditions. This robustness is essential for practical applications, ensuring reliable detection sensitivity and accuracy regardless of the specific orientation or polarization of incident light, which is critical for real-world scenarios such as cancer diagnosis.

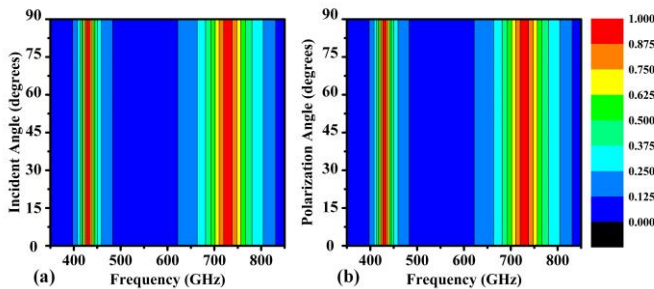


Fig. 9: The impact of angle modification on absorption rate at: (a) incidence angle, and (b) polarization angle.

Polarization can significantly affect the signal-to-noise ratio (SNR) in sensing and imaging applications, potentially leading to distorted results. The symmetrical construction recommended in references [14] and [15] aligns the sensor with polarization effects. Notably, the absorption properties remain consistent even as the polarization angle varies between  $0^\circ$  and  $90^\circ$  as shown in Fig. 9.

Fig. 9(a) shows that key absorption areas remain stable regardless of orientation, and Fig. 9(b) confirms this consistency across different angles. This stability suggests the model's effectiveness across a wide range of incidence angles and polarizations, efficiently absorbing and transferring incident energy regardless of the wave's orientation or direction.

Figs. 10 and 11 demonstrate the proposed sensor's exceptional performance, particularly in biomedical applications, due to its high electric field density. These field

distributions provide valuable insights into the resonance process and deepen our understanding of THz electromagnetic absorbers. By analysing the electric and magnetic field strengths at specific frequencies, we can better understand how the metamaterial structure contributes to signal resonances, which is essential for optimizing biosensor design.

Fig. 10 shows the electric field (E-field) distributions at resonant frequencies of 0.437 THz and 0.75 THz, revealing regions of high field intensity that are essential for efficient energy transfer to the biological medium. These high-intensity regions are a direct result of the resonator's plasmonic properties and the local enhancement of the electromagnetic field, which are critical for maximizing the interaction with target biomolecules. Identifying these regions allows for the optimization of the biosensor's design, enhancing its sensitivity by ensuring that the strongest fields are concentrated where the biological interactions occur.

Fig. 11 shows the magnetic field (H-field) distributions at the same resonant frequencies, providing insights into the magnetic response of the metamaterial structure. The H-field patterns help clarify the resonance modes, indicating how magnetic energy is stored and dissipated within the sensor. This understanding is vital for tuning the metamaterial's resonance characteristics to optimize performance.

Fig. 12 illustrates the surface current distribution at the resonant frequencies of 0.437 THz and 0.75 THz, shedding light on the electromagnetic response of the metamaterial. These distributions highlight the pathways of energy flow that underlie the observed resonant behaviour and absorption characteristics. By optimizing the surface current flow, the biosensor's sensitivity can be enhanced, enabling it to detect subtle changes in the biological environment, which is crucial for accurate and reliable diagnostics.

At 0.437 THz, Fig. 12(a) reveals parallel and antiparallel surface current patterns, indicating a strong magnetic response. The antiparallel currents form a circular pattern, suggesting robust magnetic flux in response to the incident H-field. Fig. 12(b) presents the current distribution for the second resonance mode at 0.75 THz, where the direction of current flow, whether parallel or antiparallel, directly influences the distribution of electric and magnetic fields. Parallel currents generate an internal magnetic field that opposes the external H-field, while antiparallel currents enhance the magnetic response. This analysis clarifies the physical absorption processes in the proposed metamaterial structure, providing insights critical for optimizing biosensor design.

Fig. 13 illustrates the power flow distribution within the metamaterial structure at the resonant frequencies of 0.437 THz and 0.75 THz. This analysis highlights the pathways of energy propagation and identifies regions where energy is concentrated and dissipated. Optimizing power flow is essential for improving the biosensor's sensitivity and efficiency in detecting subtle changes in biological samples. At the resonance frequency of 0.437 THz, Fig. 13(a) shows a uniform distribution of power flow, while Fig. 13(b) reveals a dense zone of energy concentration at 0.75 THz. These patterns indicate that the proposed sensor effectively absorbs incident electromagnetic waves.

The electromagnetic characteristics of the proposed dual-band micro-biosensor, designed to function as a metamaterial

> REPLACE THIS LINE WITH YOUR MANUSCRIPT ID NUMBER (DOUBLE-CLICK HERE TO EDIT) <

absorber in the 0–1 THz frequency range, are illustrated in Figs. 14 to 16. Fig. 14 presents the real and imaginary components of the permeability ( $\mu$ ) and permittivity ( $\epsilon$ ) of the metamaterial. These graphs depict the material's response to electromagnetic waves across frequencies up to 1 THz.

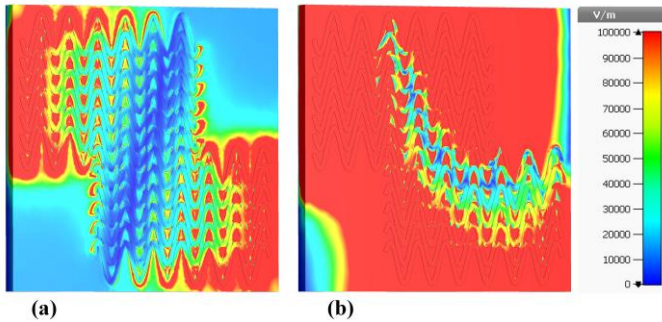


Fig. 10: Distributions of the electric field across the proposed metamaterial structure: (a) E-field at 0.437 THz, and (b) E-field at 0.75 THz.

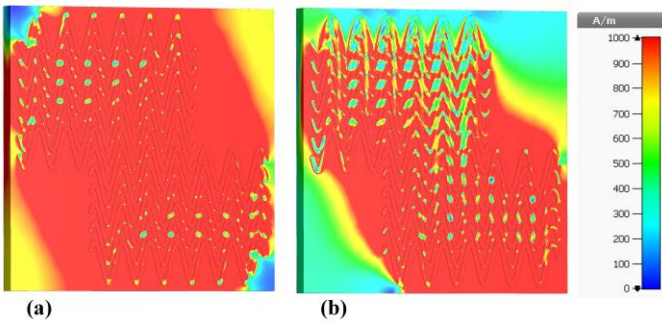


Fig. 11: An illustrated color map showing the magnetic field distribution over the proposed metamaterial structure: (a) H-field at 0.437 THz, and (b) H-field at 0.75 THz.

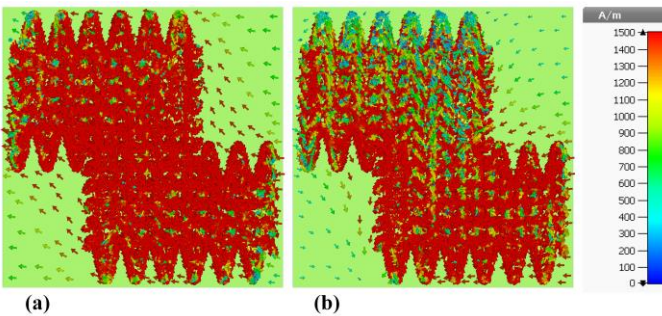


Fig. 12: The surface current distribution over the proposed metamaterial structure: (a) at 0.437 THz, and (b) at 0.75 THz.

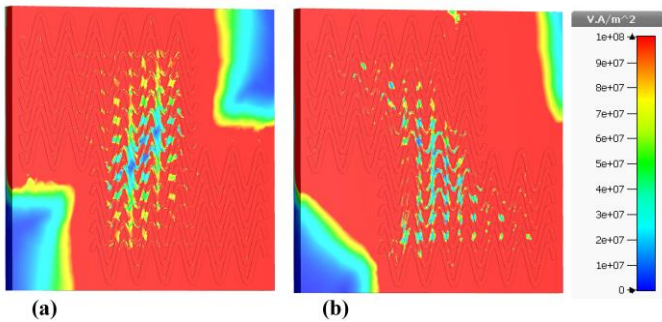


Fig. 13: Power flow over the proposed metamaterial structure: (a) at 0.437 THz, and (b) at 0.75 THz.

Fig. 14(a) presents the real parts of permittivity ( $\epsilon'$ ) and permeability ( $\mu'$ ), which correspond to the material's ability to store electric and magnetic energy, respectively. The dual-band nature of the sensor is evident from the distinct resonant peaks within this frequency range, signifying the specific frequencies where the absorber operates most effectively. These resonant peaks highlight the sensor's ability to interact strongly with electromagnetic waves at these frequencies, leading to enhanced sensitivity in detecting changes in the dielectric properties of biological tissues. Consequently, the sensor's accuracy in monitoring or diagnosing biological conditions is significantly improved, as it can respond to subtle variations in tissue properties over these dual bands.

Fig. 14(b) displays the imaginary components of permittivity ( $\epsilon''$ ) and permeability ( $\mu''$ ), which represent the material's loss factors and are crucial for understanding energy dissipation within the metamaterial. The minimal loss observed at the resonant frequencies ensures high efficiency and sensitivity, making the absorber well-suited for non-invasive diagnostic applications. The behaviour of these imaginary components confirms the material's effectiveness as a perfect absorber in the terahertz range.

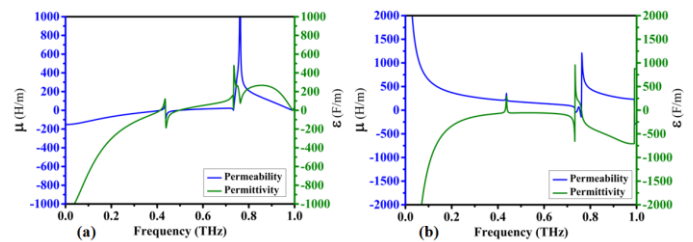


Fig. 14: Real and imaginary components of permeability ( $\mu$ ) and permittivity ( $\epsilon$ ) of the proposed metamaterial absorber: (a) Real components of  $\mu$  and  $\epsilon$ , and (b) Imaginary components of  $\mu$  and  $\epsilon$ .

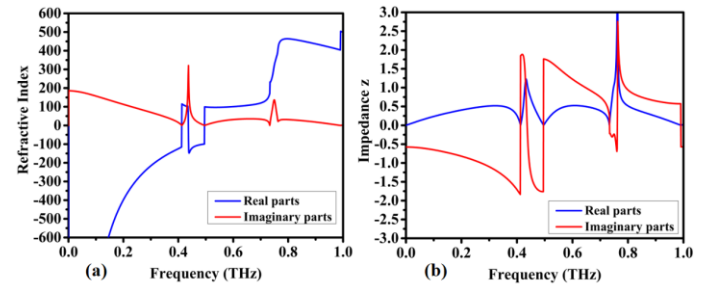


Fig. 15: The proposed metamaterial absorber characterizing responses: (a) Real and imaginary parts of the Refractive Index, and (b) Impedance ( $Z$ ).

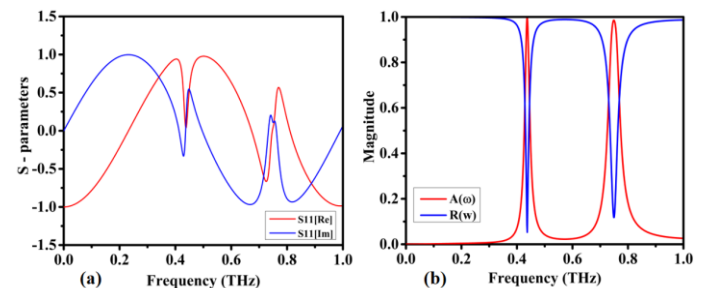


Fig. 16: The proposed metamaterial absorber's: (a) the real & imaginary parts of  $S_{11}$ , and (b) Reflection ( $R$ ) & absorption ( $A$ ) spectra.

> REPLACE THIS LINE WITH YOUR MANUSCRIPT ID NUMBER (DOUBLE-CLICK HERE TO EDIT) <

Fig. 15(a) shows the impedance characteristics, which are essential for evaluating the absorber's performance. The dual-band nature of the absorber is evident in the two frequency bands where the impedance aligns with that of free space, indicating optimal absorption. At these resonant frequencies, the sensor is highly effective at detecting changes in the electromagnetic properties of biological tissues, ensuring high sensitivity for biosensing applications.

Fig. 15(b) presents both the real and imaginary parts of the refractive index. The real part indicates how much the wave slows down within the material, while the imaginary part represents the absorption loss. Significant variations in the real part of the refractive index at the resonant frequencies underscore the sensor's dual-band capability. These variations are crucial for fine-tuning the sensor's sensitivity and ensuring accurate detection of dielectric property changes in biological tissues. Additionally, the low absorption loss in the imaginary part at these frequencies further enhances the sensor's efficiency and reliability.

Fig. 16 shows the reflection coefficient ( $S_{11}$ ), reflection, and absorption spectra of the absorber. Fig. 16(a) shows the real and imaginary parts of  $S_{11}$ , which indicate the reflection behaviour of the sensor. The dual-band characteristic is evident from the dips in the magnitude of  $S_{11}$  at two specific frequencies, where minimal reflection signifies strong resonance and efficient absorption. These resonant frequencies fall within the target terahertz range, which is crucial for the biosensor's sensitivity and accuracy.

The reflection and absorption spectra shown in Fig. 16(b) highlight two peaks in the absorption spectrum that correspond to the dual-band frequencies. These peaks represent the frequencies at which the metamaterial structure absorbs the maximum amount of incident electromagnetic energy, thereby enhancing the sensor's ability to detect changes in the dielectric constant of biological tissues. The low reflection values at these frequencies confirm the high efficiency of the absorber.

The relationship between the figures is clear, as the dual-band resonant frequencies are consistently identified across different parameters. The permeability and permittivity analysis in Fig. 14 provides the foundational material properties that influence the impedance, refractive index, and  $S_{11}$  parameter responses shown in Figs. 15 and 16. The coherence in the identified resonant frequencies across these figures validates the effectiveness of the design. These comprehensive analyses offer valuable insights for optimizing the micro-biosensor's design and functionality, ensuring effective operation within the desired terahertz frequency bands for early-stage cancer detection.

#### IV. DIAGNOSIS OF CERVICAL CANCER

The development of a biosensor for cervical cancer diagnostics is crucial for early cancer detection. The proposed metamaterial sensor is designed to identify cervical cancer by analysing its absorption spectra, providing a novel and effective approach for enhancing early detection and prevention.

Research [16]-[20] has shown that healthy cervical tissue has a refractive index of 1.368, while malignant tissue has a

slightly higher refractive index of 1.392. As illustrated in Fig. 17, the sensor can be used to detect cancerous biological tissue by placing the tissue sample between glass slides and positioning it over the metamaterial sensor. The 0–1 THz frequency range is particularly advantageous for biosensing due to its low water absorption, which allows for deeper tissue penetration. This range also provides distinct spectral fingerprints for biomolecules, facilitating the identification of specific cancer-related markers. Additionally, terahertz radiation is non-ionizing, making it safe for biological applications.

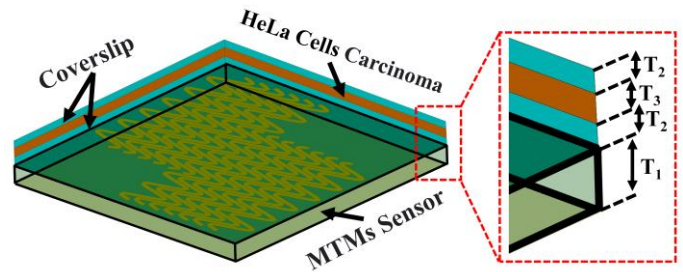


Fig. 17: A layer of biological tissue (either healthy cervical tissue or cancerous cervical tissue) is placed on top of the proposed metamaterial biosensor.

Fig. 18(a) presents the sensor's findings for healthy and cancerous cervical tissue across the 0–1 THz frequency range, with a focus on the initial peak in the 0.41 THz to 0.43 THz region. Fig. 18(b) highlights a significant difference in resonance frequency—specifically 1010 MHz—between healthy and cancerous cervical tissue.

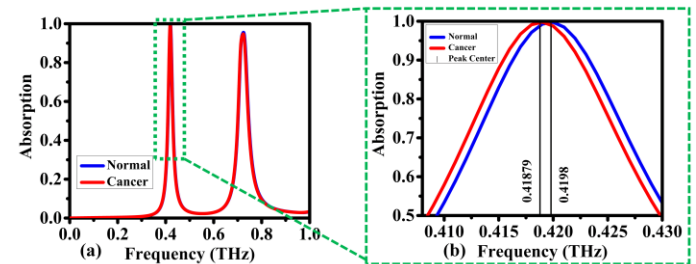


Fig. 18: Absorption coefficient of the proposed biosensor for detecting normal Cervical and Cervical cancer, (a) 0 - 1 THz, and (b) 0.41 – 0.43 THz.

Fig. 19(a) presents the detection results for both cervical cancer and normal cervical tissue, highlighting a second peak in the 0.7 to 0.75 THz range. Fig. 19(b) demonstrates a significant frequency difference of 1690 MHz between cervical cancer and healthy cervical tissue. This notable frequency distinction makes it feasible to identify cervical cancer using terahertz imaging methods.

A careful examination of the terahertz frequency spectrum of a patient's HeLa cells carcinoma, as shown in Fig. 19, allows medical professionals to accurately diagnose the presence of cervical cancer. This capability facilitates early intervention and treatment, underscoring the potential of the proposed metamaterial sensor in advancing cervical cancer diagnostics.

> REPLACE THIS LINE WITH YOUR MANUSCRIPT ID NUMBER (DOUBLE-CLICK HERE TO EDIT) <

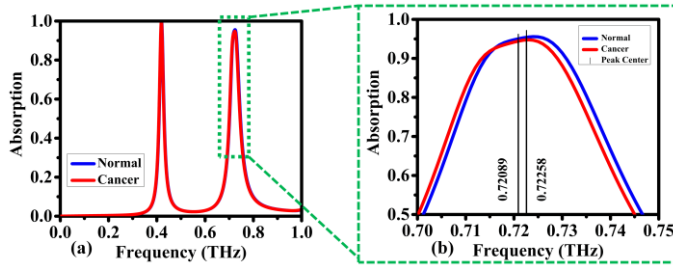


Fig. 19: Absorption coefficient of the proposed biosensor for detecting normal Cervical and Cervical cancer, (a) 0 - 1 THz, and (b) 0.7 - 0.75 THz.

When evaluating a sensor's performance, sensitivity ( $S$ ) is a critical parameter that describes its ability to detect small changes in the measured quantity. Sensitivity is generally categorized into two main types: frequency sensitivity and intensity sensitivity. Frequency sensitivity is defined as [5]:

$$S = \frac{\Delta f}{\Delta n} \quad (3)$$

Where  $\Delta f$  represents the frequency shift of the resonance peak, and  $\Delta n$  denotes the change in the refractive index (RI), typically measured in refractive index units (RIU). This type of sensitivity is crucial for detecting minute variations in the biological environment, which are indicative of pathological changes. Intensity sensitivity, on the other hand, is given by:

$$S = \frac{\Delta I}{\Delta n} \quad (4)$$

Where  $\Delta I$  indicates the change in resonant intensity. This measure is particularly important for applications that require precise quantification of analyte concentration based on intensity changes.

The figure of merit ( $FOM$ ) is another crucial attribute that quantifies a sensor's selectivity. It is defined as the ratio of sensitivity ( $S$ ) to the full width at half maximum ( $FWHM$ ) of the resonant dip, as expressed in [5]:

$$FOM = \frac{S}{FWHM} \quad (5)$$

A higher figure of merit ( $FOM$ ) indicates a more selective sensor, capable of distinguishing between small differences in the measured quantity. The quality factor ( $Q$ -factor) measures the sharpness of the resonance, which is crucial for achieving high sensitivity. It is determined by the ratio of the resonant wavelength ( $\lambda$ ) to the full width at half maximum ( $FWHM$ ):

$$Q_{factor} = \frac{\lambda}{FWHM} \quad (6)$$

In terahertz (THz) sensing, metamaterial-based biosensors leverage high  $Q$ -factors and sensitivity metrics to achieve enhanced detection capabilities. The unique electromagnetic properties of metamaterials contribute to significant improvements in both sensitivity and figure of merit ( $FOM$ ), making them highly effective for applications such as early cancer detection and other biomedical diagnostics. By optimizing sensitivity,  $FOM$ , and  $Q$ -factor, THz metamaterial-

based biosensors can deliver superior performance, enabling precise and early detection of biological changes. This underscores their potential as powerful tools in medical diagnostics and various sensing applications [21][22].

Table 2 presents a comparative analysis of the proposed metamaterial biosensor alongside previously reported systems in the literature. All these systems utilize the phase change of terahertz waves to obtain data on material properties. Specifically, these sensors exploit changes in the refractive index to affect absorption spectra, a principle that this study applies to differentiate between healthy and cancerous tissue.

The urgent need for early identification and effective treatment of cervical cancer highlights the importance of accurately distinguishing malignant tissue. In terms of performance, particularly absorptivity, the proposed biosensor compares favourably with benchmark devices. Additionally, it features a compact physical size, which is crucial for practical applications, such as needing smaller biopsy samples for diagnostics.

TABLE 2: COMPARISON BETWEEN OTHER METAMATERIAL-BASED SENSORS AND THE PROPOSED BIOSENSOR

Ref.	Techniques used	Frequency operating (THz)	Material substrate	Absorptivity	Application
[23]	Au/ Dielectric Teflon/Au	1-2.2	dielectric Teflon	0.99	Sensor
[24]	Graphene/ Topas/Au	0.5-4.5	Topas spacer	0.99, 0.98, 0.99	Ultra-Broadband Absorber
[25]	Gold/Silicon Dioxide/ Gold	1.5-1.7	silicon dioxide	0.972, 0.991	Biosensor for Detecting Corona Virus
[26]	Bulk Dirac Semimetal/ Photonic Crystal/Au	1-3	photonic crystal plate	0.97, 0.98, 0.99	Narrowband Perfect Absorber
[27]	Graphene/ Au/ SiO <sub>2</sub> /Au	2-6	SiO <sub>2</sub>	0.99	Refractive Index Sensor
[28]	Au/SiO <sub>2</sub> / Graphene	7-9.5	SiO <sub>2</sub>	0.98	Multi-Frequency Broadband and Ultra-Broadband
[29]	Ion Gel/ Graphene/ Teflon/Gold	0.7-5	Teflon	>0.96	Polarization-Sensitive
[30]	PET/FSS/UV glue/ Graphene	0-3	PET	0.99, 0.80, 0.95	Multifunctional Tunable Terahertz
[31]	Au/dielectric layer/Au	1-3	dielectric layer	0.99, 0.99	Sensor
[32]	Glass/InSb/ MgF <sub>2</sub> /InSb	0-0.37	Glass	0.998	Colon Cancer Detection
[33]	SiO <sub>2</sub> / Graphene	0.5-2.5	SiO <sub>2</sub>	-	Breast Cancer Detection
This work	Al/PET/Al	0-1	PET	0.9977, 0.984	Biosensor, Cervical Cancer Diagnostics and Microwave Imaging

Fig. 20 illustrates the application of the proposed biosensor, showing the testing of a cervical sample placed on a coverslip. Fig. 21(a) depicts a normal cervical scan, which reveals a weak electric field. In contrast, Fig. 21(b) shows an area of red, indicating a very high electric field density, characteristic of cancerous tissue. Further distinction is provided by examining the electric field at the second peak of 0.75 THz, as shown in Fig. 22. Fig. 22(a) presents a region with a very low electric field, corresponding to a healthy cervix, while Fig. 22(b) shows a region with high electric field density, indicative of cervical cancer.



> REPLACE THIS LINE WITH YOUR MANUSCRIPT ID NUMBER (DOUBLE-CLICK HERE TO EDIT) <

To validate these electric field findings, a parallel examination of the magnetic field is conducted, as demonstrated in Fig. 23. The results from detecting the H-field are consistent with the electric field observations, reinforcing the reliability and effectiveness of the proposed metamaterial biosensor in distinguishing between healthy and cancerous cervical tissue.

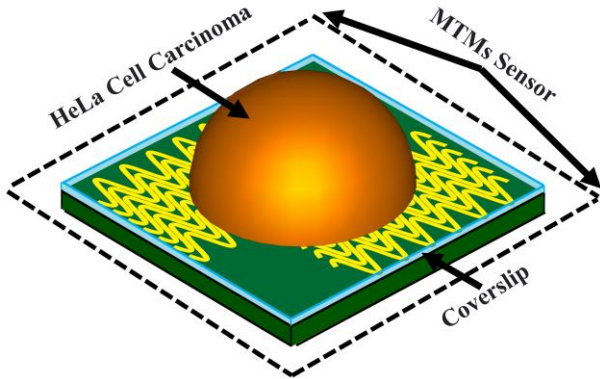


Fig. 20: The diagnosis of cervical cancer using the MWI approach.

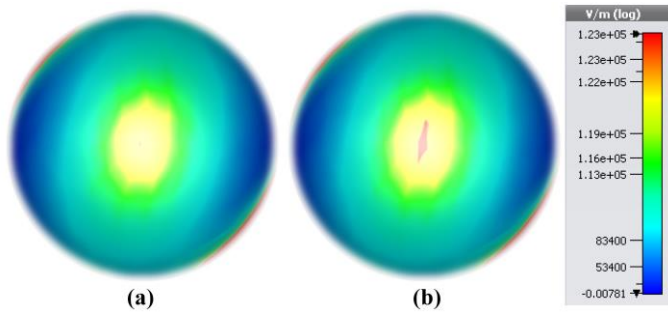


Fig. 21: The E-field distribution of biological tissue sample at 0.437 THz: (a) healthy cervical, and (b) cervical cancer.

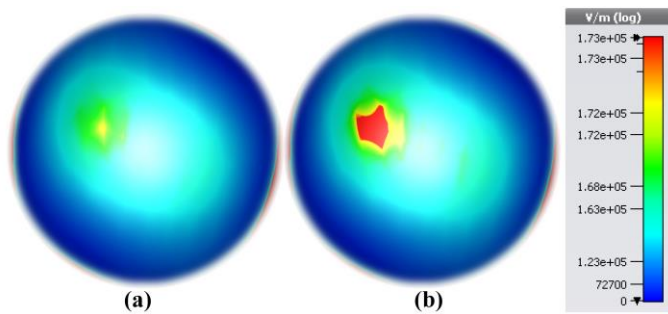


Fig. 22: The E-field distribution of biological tissue sample at 0.75 THz: (a) healthy cervical, and (b) cervical cancer.

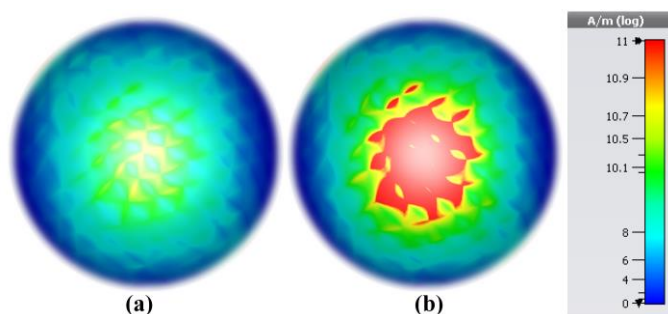


Fig. 23: The H-field distribution of biological tissue sample at 0.437 THz: (a) healthy cervical, and (b) cervical cancer.

## V. FUTURE PERSPECTIVE

These results demonstrate that early-stage diagnosis of various cancers, including breast cancer, colon cancer, adrenal gland cancer (such as PC-12 tumors), and non-melanoma skin cancer, can be significantly enhanced using terahertz electromagnetic wave imaging biosensors. These advanced biosensors utilize THz EM waves to detect subtle changes in tissue properties that are indicative of cancerous growth.

Terahertz imaging is particularly advantageous for early cancer detection due to its ability to penetrate biological tissues with minimal damage and its sensitivity to variations in tissue composition and structure. By analyzing the interaction of THz waves with different types of tissues, these biosensors can identify specific signatures associated with early-stage tumors, improving diagnostic accuracy and enabling timely intervention.

For breast cancer, THz imaging can reveal abnormal tissue changes before they become visible through traditional imaging techniques. Similarly, for colon cancer, THz biosensors can detect precancerous lesions and early-stage tumors by differentiating between healthy and malignant tissue based on their unique THz absorption and reflection characteristics.

In the case of adrenal gland cancer (PC-12), THz imaging can be used to distinguish between benign and malignant lesions, facilitating early diagnosis and appropriate treatment planning. Non-melanoma skin cancer detection benefits from THz imaging's ability to differentiate between cancerous and healthy skin tissues with high precision.

Overall, the use of THz electromagnetic wave imaging biosensors offers a promising approach for early cancer detection across various types of cancers, enhancing diagnostic capabilities and potentially improving patient outcomes through earlier intervention and more accurate monitoring.

## VI. BENCHMARKING

The proposed terahertz dual-band metamaterial biosensor represents a significant advancement over traditional microwave imaging techniques for cervical cancer diagnostics. This biosensor, designed as a metamaterial perfect absorber, operates within the 0-1 THz range and exhibits dual-band functionality. It achieves impressive absorption rates of 99.77% and 98.4% at its first and second resonant peaks, respectively (see Table 2).

Table 3 compares the performance metrics of the proposed biosensor with other metamaterial-based biosensors, showing that it has a sensitivity of 0.042 THz/RIU at the first peak and 0.0704 THz/RIU at the second peak, with quality factors (Q-factors) of 20.382 and 16.286, respectively. The figures of merit (FOM) for the proposed biosensor are 1.9589 RIU<sup>-1</sup> and 1.529 RIU<sup>-1</sup> at these peaks, indicating its high precision and efficiency.

Unlike conventional sensors, the compact size of this metamaterial biosensor allows for the use of significantly smaller biopsy samples, facilitating less invasive testing procedures. Its high sensitivity and specificity are crucial for

> REPLACE THIS LINE WITH YOUR MANUSCRIPT ID NUMBER (DOUBLE-CLICK HERE TO EDIT) <

early-stage cancer detection, ensuring accurate identification of abnormalities in biological tissues. The superior performance metrics of this biosensor, coupled with its practical advantages, highlight its potential as a highly effective tool for non-invasive cervical cancer diagnostics.

TABLE 3: COMPARISON OF THE PROPOSED BIOSENSOR'S PERFORMANCE METRICS WITH OTHER METAMATERIAL-BASED BIOSENSORS

Ref.	Year Published	FOM (RIU <sup>-1</sup> )	Q	S (THz/RIU)	Bio-application
[34]	2017	-	-	0.0242, 0.02438	Detection of Virus
[35]	2021	-	-	0.074	Cervical cancer
[36]	2022	-	-	0.068	Hepatocellular Carcinoma Sensor
[37]	2022	1.81, 1.57	8.21, 6.05	0.203	Bovine Serum Albumin Protein
[38]	2023	-	11	0.278	Non-Melanoma Skin Cancer Diagnostics
[39]	2023	0.86, 1.15	12.8, 13.5	0.0515, 0.076	Cervical Cancer Diagnostics
This work	-	1.9589, 1.529	20.382, 16.286	0.042, 0.0704	

FOM: Figure of merit, RIU-I: Refractive index unit

## VII. CONCLUSIONS

This research highlights the potential of utilizing metamaterial structures as biosensors for the early detection of cancerous biological tissues. The underlying mechanism is based on the ability of cancerous cells to alter the effective dielectric constant of the surrounding tissue. This alteration leads to a shift in the resonance frequency of the metamaterial sensor, enabling the detection of cancerous changes at an early stage.

One of the key advantages of the proposed metamaterial biosensor is its compact size. Unlike traditional sensors, which often require larger sample sizes, this sensor's dimensions are independent of the wavelength, allowing it to analyze significantly smaller biopsy samples. This compact nature not only reduces the invasiveness of the procedure but also improves patient comfort.

Furthermore, the biosensor has demonstrated effectiveness in identifying abnormalities within biological tissues, providing a valuable tool for early cancer detection. The ability to detect subtle changes in tissue properties makes it particularly useful for monitoring and diagnosing various forms of cancer at a stage when treatment options are most effective.

Overall, this research underscores the promising capabilities of metamaterial-based biosensors in enhancing diagnostic accuracy and facilitating earlier intervention in cancer treatment. The compact design and high sensitivity of the biosensor contribute to its potential as a powerful tool for advancing medical diagnostics.

## VIII. USE OF HUMAN PARTICIPANTS

There were no humans involved in the study.

## IX. COMPETING INTERESTS

The authors declare no competing interests.

## X. DATA AVAILABILITY

The datasets used and/or analyzed during the current study are available from the first author on reasonable request.

## XI. AUTHOR CONTRIBUTIONS

Conceptualization: M.N.H. (Musa N. Hamza), M.A. (Mohammad Alibakhshikenari), B.V. (Bal Virdee), M.H. (Muhamad A. Hamad) & S.Kh. (Salahuddin Khan); Data curation: M.N.H. & S.K. (Slawomir Koziel); Formal analysis: M.N.H. & B.V.; Visualization: M.N.H., M.A, S.Kh. and S.K.; Writing—original draft: M.N.H., M.A, B.V., M.H. and S.K.; Writing—review and editing: M.A, B.V., S.Kh., S.K, and E.L.; Software: M.N.H.; Resources: M.N.H., M.A, M.H. and S.K.; Supervision: M.A, B.V. and S.K.

## REFERENCES

- [1] H. Sung *et al.*, "Global Cancer Statistics 2020: GLOBOCAN Estimates of Incidence and Mortality Worldwide for 36 Cancers in 185 Countries," (in eng), *CA Cancer J Clin*, vol. 71, no. 3, pp. 209-249, May 2021.
- [2] H. Udagawa *et al.*, "Liposomal eribulin for advanced adenoid cystic carcinoma, gastric cancer, esophageal cancer, and small cell lung cancer," (in eng), *Cancer Med*, vol. 12, no. 2, pp. 1269-1278, Jan 2023.
- [3] F. Bray, J. Ferlay, I. Soerjomataram, R. L. Siegel, L. A. Torre, and A. Jemal, "Global cancer statistics 2018: GLOBOCAN estimates of incidence and mortality worldwide for 36 cancers in 185 countries," (in eng), *CA Cancer J Clin*, vol. 68, no. 6, pp. 394-424, Nov 2018.
- [4] P. U. Jepsen, D. G. Cooke, and M. Koch, "Terahertz spectroscopy and imaging – Modern techniques and applications," *Laser & Photonics Reviews*, vol. 5, no. 1, pp. 124-166, 2011.
- [5] A. H. Aly, A. A. Ameen, M. A. Mahmoud, Z. S. Matar, M. Al-Dossari, and H. A. Elsayed, "Photonic Crystal Enhanced by Metamaterial for Measuring Electric Permittivity in GHz Range," *Photonics*, vol. 8, no. 10, p. 416, 2021.
- [6] A. Siemion, L. Minkevičius, L. Qi, and G. Valušis, "Spatial filtering based terahertz imaging of low absorbing objects," *Optics and Lasers in Engineering*, vol. 139, p. 106476, 2021/04/01/ 2021.
- [7] Liu, H., Zhang, S., & Han, J., "Microwave sensing using metamaterial absorbers." *Applied Physics Letters*, vol.99, no.17, 174101, 2011.
- [8] Landy, N. I., Sajuyigbe, S., Mock, J. J., Smith, D. R., & Padilla, W. J. "Perfect Metamaterial Absorber." *Physical Review Letters*, vol.100, no. 20, 207402, 2008.
- [9] Al-Naib, I. A., Jansen, C., & Koch, M. (2013). "High-Q terahertz resonances in all-dielectric metamaterials." *Applied Physics Letters*, 103(10), 101101.
- [10] B. Liu *et al.*, "Terahertz ultrasensitive biosensor based on wide-area and intense light-matter interaction supported by QBIC," *Chemical Engineering Journal*, vol. 462, p. 142347, 2023.
- [11] Y. Peng *et al.*, "Three-step one-way model in terahertz biomedical detection," *Photonix*, vol. 2, pp. 1-18, 2021.
- [12] M. Askari, H. Pakarzadeh, and F. Shokrgozar, "High Q-factor terahertz metamaterial for superior refractive index sensing," *JOSA B*, vol. 38, no. 12, pp. 3929-3936, 2021.
- [13] O. Ramadan, "Stability-Improved ADE-FDTD Implementation of Drude Dispersive Models," *IEEE Antennas and Wireless Propagation Letters*, vol. 17, no. 5, May 2018, pp.877-880.
- [14] S. Li *et al.*, "A polarization-independent fiber-optic SPR sensor," *sensors*, vol. 18, no. 10, p. 3204, 2018.
- [15] M. Abdelsalam, A. M. Mahmoud, and M. A. Swillam, "Polarization independent dielectric metasurface for infrared beam steering applications," *Scientific Reports*, vol. 9, no. 1, p. 10824, 2019.
- [16] K. Ahmed, B. K. Paul, F. Ahmed, M. A. Jabin, and M. S. Uddin, "Numerical demonstration of triangular shaped photonic crystal fibre-based biosensor in the Terahertz range," *IET Optoelectronics*, vol. 15, no. 1, pp. 1-7, 2021.
- [17] M. A. Jabin *et al.*, "Surface plasmon resonance based titanium coated biosensor for cancer cell detection," *IEEE Photonics Journal*, vol. 11, no. 4, pp. 1-10, 2019.

> REPLACE THIS LINE WITH YOUR MANUSCRIPT ID NUMBER (DOUBLE-CLICK HERE TO EDIT) <

- [18] P. Kumar, V. Kumar, and J. S. Roy, "Dodecagonal photonic crystal fibers with negative dispersion and low confinement loss," *Optik*, vol. 144, pp. 363-369, 2017.
- [19] T. Parvin, K. Ahmed, A. M. Alatwi, and A. N. Z. Rashed, "Differential optical absorption spectroscopy-based refractive index sensor for cancer cell detection," *Optical Review*, vol. 28, pp. 134-143, 2021.
- [20] P. Sharma, P. Sharan, and P. Deshmukh, "A photonic crystal sensor for analysis and detection of cancer cells," in *2015 International conference on pervasive computing (ICPC)*, 2015, pp. 1-5: IEEE.
- [21] M. Gómez-Castaño, J. L. Garcia-Pomar, L. A. Pérez, S. Shanmugathan, S. Ravaine, and A. Mihi, "Electrodeposited negative index metamaterials with visible and near infrared response," *Advanced Optical Materials*, vol. 8, no. 19, p. 2000865, 2020.
- [22] R. Krause *et al.*, "Ultrafast charge separation in bilayer WS<sub>2</sub>/graphene heterostructure revealed by time-and angle-resolved photoemission spectroscopy," *Frontiers in Physics*, vol. 9, p. 668149, 2021.
- [23] A. S. Saadeldin, M. F. O. Hameed, E. M. Elkaramany, and S. S. Obayya, "Highly sensitive terahertz metamaterial sensor," *IEEE Sensors Journal*, vol. 19, no. 18, pp. 7993-7999, 2019.
- [24] L. Liu, W. Liu, and Z. Song, "Ultra-broadband terahertz absorber based on a multilayer graphene metamaterial," *Journal of Applied Physics*, vol. 128, no. 9, 2020.
- [25] Z. El-Wasif, T. Ismail, and O. Hamdy, "Design and optimization of highly sensitive multi-band terahertz metamaterial biosensor for coronaviruses detection," *Optical and Quantum Electronics*, vol. 55, no. 7, p. 604, 2023.
- [26] Y. Wang *et al.*, "Terahertz tunable three band narrowband perfect absorber based on Dirac semimetal," *Physica E: Low-dimensional Systems and Nanostructures*, vol. 131, p. 114750, 2021.
- [27] M.-R. Nickpay, M. Danaie, and A. Shahzadi, "Highly sensitive THz refractive index sensor based on folded split-ring metamaterial graphene resonators," *Plasmonics*, pp. 1-12, 2021.
- [28] Z. Chen *et al.*, "Graphene Multi-Frequency Broadband and Ultra-Broadband Terahertz Absorber Based on Surface Plasmon Resonance," *Electronics*, vol. 12, no. 12, p. 2655, 2023.
- [29] S. Asgari and T. Fabritius, "Numerical Simulation and Equivalent Circuit Model of Multi-Band Terahertz Absorber Composed of Double-Sided Graphene Comb Resonator Array," *IEEE Access*, vol. 11, pp. 36052-36063, 2023.
- [30] S. Zhuang *et al.*, "Graphene-Based Absorption-Transmission Multi-Functional Tunable THz Metamaterials," *Micromachines*, vol. 13, no. 8, p. 1239, 2022.
- [31] B.-X. Wang, Y. He, P. Lou, and W. Xing, "Design of a dual-band terahertz metamaterial absorber using two identical square patches for sensing application," *Nanoscale Advances*, vol. 2, no. 2, pp. 763-769, 2020.
- [32] Z. Vafapour, W. Troy, and A. Rashidi, "Colon cancer detection by designing and analytical evaluation of a water-based THz metamaterial perfect absorber," *IEEE Sensors Journal*, vol. 21, no. 17, pp. 19307-19313, 2021.
- [33] C. Tan *et al.*, "Cancer Diagnosis Using Terahertz-Graphene-Metasurface-Based Biosensor with Dual-Resonance Response," *Nanomaterials*, vol. 12, no. 21, p. 3889, 2022.
- [34] S. Park, S. Cha, G. Shin, and Y. Ahn, "Sensing viruses using terahertz nano-gap metamaterials," *Biomedical optics express*, vol. 8, no. 8, pp. 3551-3558, 2017.
- [35] D. Li *et al.*, "Identification of early-stage cervical cancer tissue using metamaterial terahertz biosensor with two resonant absorption frequencies," *IEEE Journal of Selected Topics in Quantum Electronics*, vol. 27, no. 4, pp. 1-7, 2021.
- [36] R. Bhati and A. K. Malik, "Ultra-efficient terahertz metamaterial sensor," *Results in Optics*, vol. 8, p. 100236, 2022.
- [37] H. Hu, B. Qi, Y. Zhao, X. Zhang, Y. Wang, and X. Huang, "A graphene-based THz metasurface sensor with air-spaced structure," *Frontiers in Physics*, vol. 10, p. 990126, 2022.
- [38] Y. Shen *et al.*, "Low-Concentration Biological Sample Detection Using an Asymmetric Split Resonator Terahertz Metamaterial," in *Photonics*, vol. 10, no. 2, p. 111: MDPI, 2023.
- [39] M. N. Hamza and M. T. Islam, "Designing an Extremely Tiny Dual-Band Biosensor Based on MTMs in the Terahertz Region as a Perfect Absorber for Non-Melanoma Skin Cancer Diagnostics," *IEEE Access*, vol. 11, pp. 136770-136781, 2023.



**Musa N. Hamza** received the B.Sc. degree from the Department of Physics, Faculty of Science and Health, Koya University, Koysinjaq, Erbil, Iraqi Kurdistan, Iraq, in 2015, and the M.Sc. degree from the Department of Medical Physics, College of Medical and Applied Sciences, Charmo University, Chamchamal, Sulaymaniyah, in 2023. His research interests include medical physics, the diagnosis of

different types of cancer at an early stage, antenna arrays, metamaterials, sensors, and biosensors.



**Mohammad Alibakhshkenari** (Member, IEEE) was born in Mazandaran, Iran, in February 1988. He received the Ph.D. degree with the European label in electronics engineering from the University of Rome "Tor Vergata" (UNITOV), Italy, in February 2020. From May to December 2018, he was a Ph.D. visiting researcher at the Chalmers University of Technology, Gothenburg,

Sweden. His training during this visit included a research stage in the Swedish Company "Gap Waves AB". During his Ph.D. program (Nov. 2016 – Feb. 2020), he has attended thirteen European Doctoral Schools organized by various European universities and organizations, and he successfully achieved all the credits leading him to obtain his Ph.D. degree with the European label. In November 2019 he was winner of a postdoctoral research fund for two years awarded by the UNITOV, Italy. Between July 2021 to August 2024, he was with the Department of Signal Theory and Communications, Universidad Carlos III de Madrid (uc3m), Spain, as a Principal Investigator of the CONEX (CONNECTING EXcellence)-Plus Talent Training Program and Marie Skłodowska-Curie Actions. During this Program he has spent two secondments at the (i) Microwave Engineering Center for Space Applications (MECSA), Rome, Italy, between April to August 2024, and (ii) SARAS Technology Ltd Company, Leeds, UK, between December 2022 to May 2023. In addition, during this Program he had some short research visits at the (i) University of Catania, Italy, in May 2024 along with an invited lecture entitled "Terahertz Antennas based on Metasurface and SIW" for master and PhD students, and postdoctoral researchers; (ii) University of Messina, Italy, in May 2024; (iii) University of Bradford, UK, in May 2023; (iv) Edinburgh Napier University, UK, in April 2023. For academic year 2021–2022, he received the "Teaching Excellent Acknowledgement" certificate for the course of "electromagnetic fields" from the Vice-Rector of studies of uc3m. In September 2024, he joined UNITOV, Italy, as a senior researcher. His main research interests are "electromagnetic systems, antennas and wave-propagations, metamaterials and metasurfaces, sensors, synthetic aperture radars (SAR), 5G and beyond wireless communications, multiple input multiple output (MIMO) systems, RFID tag antennas, substrate integrated waveguides (SIWs), impedance matching circuits, microwave components, millimeter-waves and terahertz integrated circuits, gap waveguide technology, beamforming matrix, and reconfigurable intelligent surfaces (RIS)", leading him to publish eight book chapters, more than 150 research articles in scientific journals, and more than 100 research papers in international conferences including 47 in-person presentations in 29 conferences and 26 on-line presentations in 12 conferences. His research works received more than 6500 citations with H-index above 50 reported by Scopus, Google Scholar, and ResearchGate. He was a recipient of the two Young Engineer Awards of the 47<sup>th</sup> and 48<sup>th</sup> European Microwave Conferences held in Nuremberg, Germany, in 2017, and in Madrid, Spain, in 2018, respectively. In April 2020, his research article entitled "High-Gain Metasurface in Polyimide On-Chip Antenna Based on CRLH-TL for Sub Terahertz Integrated Circuits," *Scientific Reports*, volume 10, Article number 4298 (2020) was awarded as the Best Month Paper at the University of Bradford, UK. He is the editor of the book project entitled "Ultra-Wideband Technologies - Diverse Techniques and Applications" to be published by IntechOpen. In addition, he serves the role of an Associate Editor for two scientific journals of (i) *Radio Science*, and (ii) *IET Journal of Engineering*. He acts as a referee in several journals and session chair in several international conferences. In addition, he is member of the reviewer panel of (i) The Dutch Research Council (NWO), (ii) The UK Research and Innovation (UKRI) Funding Service, the External examiner of several PhD dissertations from various universities.

> REPLACE THIS LINE WITH YOUR MANUSCRIPT ID NUMBER (DOUBLE-CLICK HERE TO EDIT) <



**Bal S. Virdee** (SM'08) received the B.Sc. and MPhil degrees in Communications Engineering from the University of Leeds, UK, and his Ph.D. in Electronic Engineering from the University of London, UK. He has worked in industry for various companies including Philips (UK) as an R&D-engineer and Teledyne Defence and Space as a future products developer in RF/microwave communications. He has taught at several academic institutions before joining London Metropolitan

University where he is a Senior Professor of Communications Technology in the School of Computing and Digital Media where he is Head of the Communications Technology Research Center. His research, in collaboration with industry and academia, is in wireless communications encompassing mobile-phones to satellite-technology. Prof. Virdee has chaired technical sessions at IEEE international conferences and published numerous research papers. He is Executive Member of IET's Technical and Professional Network Committee on RF/Microwave-Technology. He is a Fellow of IET and a Senior-Member of IEEE.



**Muhamad Abdullah Hamad**, currently an Assistant Professor at the University of Salahaddin in Hawler, Kurdistan Region, Iraq, has forged a distinguished career in physics. With a Ph.D. in Science (Molecular Physics) from Baghdad University, he specialized in the 'Self-assembly Fabrication of Photonic Crystals' under the guidance of Prof. Dr. Baha Tuhma Jiad. Dr. Hamad began his academic journey with a bachelor's in physics in 1989-1990 and later earned a master's in

physics in 2000, focusing on a theoretical study of background Gamma radiation for Erbil city below 3 MeV. Since joining the University of Salahaddin in 2000 as an Assistant Lecturer, he has steadily progressed, becoming a Lecturer in 2009 and attaining his current position in 2019.



**Slawomir Koziel** received the M.Sc. and Ph.D. degrees in electronic engineering from Gdansk University of Technology, Poland, in 1995 and 2000, respectively. He also received the M.Sc. degrees in theoretical physics and in mathematics, in 2000 and 2002, respectively, as well as the PhD in mathematics in 2003, from the University of Gdansk, Poland. He is currently a Professor with the Department of Engineering, Reykjavik University, Iceland. His

research interests include CAD and modeling of microwave and antenna structures, simulation-driven design, surrogate-based optimization, space mapping, circuit theory, analog signal processing, evolutionary computation and numerical analysis.



**Ernesto Limiti** (S'87-M'92-SM'17) is a full professor of Electronics in the Engineering Faculty of the University of Roma Tor Vergata since 2002, after being research and teaching assistant (since 1991) and associate professor (since 1998) in the same University. Ernesto Limiti represents University of Roma Tor Vergata in the governing body of the MECSA (Microwave Engineering Center for Space Applications), an inter-university center among several Italian

Universities. He has been elected to represent the Industrial Engineering sector in the Academic Senate of the University for the period 2007-2010 and 2010-2013. Ernesto Limiti is actually the president of the Consortium "Advanced research and Engineering for Space", ARES, formed between the University and two companies. Further, he is actually the president of the Laurea and Laurea Magistrale degrees in Electronic Engineering of the University of Roma Tor Vergata. The research activity of Ernesto Limiti is focused on three main lines, all of them belonging to the microwave and millimetre-wave electronics research area. The first one is related to characterisation and modelling for active and passive microwave and millimetre-wave devices. Regarding active devices, the research line is oriented to the small-signal, noise and large signal modelling. Regarding passive devices, equivalent-circuit models have been developed for interacting discontinuities in microstrip, for typical MMIC passive components (MIM capacitors) and to waveguide/coplanar waveguide transitions analysis and design. For active devices, new methodologies have been developed for the noise characterisation and the subsequent modelling, and equivalent-circuit

modelling strategies have been implemented both for small and large-signal operating regimes for GaAs, GaN, SiC, Si, InP MESFET/HEMT devices. The second line is related to design methodologies and characterisation methods for low noise circuits. The focus is on cryogenic amplifiers and devices. Collaborations are currently ongoing with the major radioastronomy institutes all around Europe within the frame of FP6 and FP7 programmes (RadioNet). Finally, the third line is in the analysis methods for nonlinear microwave circuits. In this line, novel analysis methods (Spectral Balance) are developed, together with the stability analysis of the solutions making use of traditional (harmonic balance) approaches. The above research lines have produced more than 250 publications on refereed international journals and presentations within international conferences. Ernesto Limiti acts as a referee of international journals of the microwave and millimetre wave electronics sector and is in the steering committee of international conferences and workshops. He is actively involved in research activities with many research groups, both European and Italian, and he is in tight collaborations with high-tech italian (Selex - SI, Thales Alenia Space, Rheinmetall, Elettronica S.p.A., Space Engineering ...) and foreign (OMMIC, Siemens, UMS, ...) companies. He contributed, as a researcher and/or as unit responsible, to several National (PRIN MIUR, Madess CNR, Agenzia Spaziale Italiana) and international (ESPRIT COSMIC, Manpower, Edge, Special Action MEPI, ESA, EUROPA, Korrigan, RadioNet FP6 and FP7 ...) projects. Regarding teaching activities, Ernesto Limiti teaches, over his istitutional duties in the frame of the Corso di Laurea Magistrale in Ingegneria Elettronica, "Elettronica per lo Spazio" within the Master Course in Sistemi Avanzati di Comunicazione e Navigazione Satellitare. He is a member of the committee of the PhD program in Telecommunications and Microelectronics at the University of Roma Tor Vergata, tutoring an average of four PhD candidates per year.